

Supporting Information for

pH-dependent Photocatalytic Performance of Modified Bismuth Vanadate by Bismuth Ferrite

Meysam Tayebi¹, Ahmad Tayyebi¹, Tayyebeh Soltani, Byeong-Kyu Lee*

Department of Civil and Environmental Engineering, University of Ulsan, Nam-gu, Daehak-ro
93, Ulsan 44610, Republic of Korea

¹:Equal contributions

2.1. Chemicals and materials

Bismuth nitrate ($\text{Bi}(\text{NO}_3)_3 \cdot 5\text{H}_2\text{O}$, Fluka), iron nitrate ($\text{Fe}(\text{NO}_3)_3 \cdot 9\text{H}_2\text{O}$, DAE), acetylacetone ($\text{C}_5\text{H}_8\text{O}_2$, Fluka), acetic acid (CH_3COOH , 99.70%, DAE) and hydrogen peroxide (30 %, H_2O_2 , DAE) were purchased and used without further purification. Ethylene glycol (EG), vanadyl acetylacetonate ($\text{C}_{10}\text{H}_{14}\text{O}_5\text{V}$) and TC were purchased from Merck. Ethanol was used without further purification and water was double distilled and deionized.

2.4. Characterization and equipment

Nanocrystalline X-ray diffraction (XRD) analysis was performed (Bruker D8Advance) with monochromatic Cu $K\alpha$ radiation ($\lambda=1.5406 \text{ \AA}$) in the 2θ range of $10\text{--}80^\circ$ at room temperature (RT). The morphology of the nanoparticles (NPs) was characterized with the aid of a scanning electron microscope (SEM; Model Quanta 250 FEG, Field Emission Gun). Raman spectra were examined using a labRam HR micro-Raman spectrophotometer (Bruker, model: Senteraa 2009, Germany) with the 785 nm laser line as an excitation source at RT. The chemical states of the elements in the samples were investigated using X-ray

photoelectron spectroscopy (XPS) data recorded on a Thermo Scientific Sigma Probe spectrometer with a monochromatic AlK α source (photon energy 1486.6 eV), spot size 400 μm , pass energy of 200 eV and energy step size of 1.0 eV. Fourier Transform Infrared (FTIR) transmittance spectra of the BVO and BVO/BFO NCs in the region 400–4000 cm^{-1} were recorded on a Perkin–Elmer Nicolet Nexus 470 FTIR spectrometer. The optical properties of the products were analyzed with a UV–vis–NIR spectrophotometer (Perkin Elmer UV-Vis-NIR model Lambda 950). The TC concentration at λ_{max} of 365 nm was measured by using a Genesis 10S UV-Vis spectrophotometer. The samples were sonicated using an ultrasonic bath (Branson 5210, Branson Ultrasonic Cleaner, USA) at a frequency of 40 kHz.

2.5. Photocatalytic activity test

Photocatalytic activity test for photodegradation experiments are described in the supplementary information.

2.2.1. Preparation of BFO MNPs

For the synthesis of pure BFO magnetic NPs (MNPs), 15 mmol of $\text{Bi}(\text{NO}_3)_3 \cdot 5\text{H}_2\text{O}$ was dissolved in 30 ml EG, and stirred for 30 min to obtain a transparent solution. A stoichiometric proportion of $\text{Fe}(\text{NO}_3)_3 \cdot 9\text{H}_2\text{O}$ with pre-existing conditions was then added and further stirred for 25 min to produce a dark red sol. This precursor was used for spin coating to prepare BFO and BVO/BFO electrodes.

To synthesize BFO NPs for photocatalytic degradation experiments, 50 mL of the BFO precursor was transferred to 80 mL Teflon line autoclave and heated at 200 °C for 4 h. The obtained reddish solution was washed with acetone and ethanol to remove any remaining EG and calcined at 450 °C for 1 h.

2.2.2. Preparation of BVO

In order to prepare the BVO precursor solution, a mixture of bismuth nitrate hexahydrate ($\text{BiN}_3\text{O}_9 \cdot 5\text{H}_2\text{O}$, 99.99% Aldrich) and vanadyl acetylacetonate ($\text{C}_{10}\text{H}_{14}\text{O}_5\text{V}$, 98% Aldrich) was added with the same mole ratio (0.1 M) to a solution of acetylacetonone ($\text{C}_5\text{H}_8\text{O}_2$, Fluka) and acetic acid (CH_3COOH , 99.70%, DAE). After sonication for 30 min, a dark green solution was obtained. Then, 50 mL of the BVO precursor was transferred to 80 mL Teflon line autoclave and heated at 200 °C for 4 h. The obtained reddish solution was washed and calcined with the same method as the BFO MNPs preparation.

2.2.3. Preparation of BFO/BVO nanocomposite (NC)

The BFO/BVO NCs were prepared by a facile solvothermal method. After 25 mL of the BVO precursor was added to 25 mL of the BFO precursor and stirred for 30 min vigorously, the mixed solution was transferred into an autoclave and heated at 200 °C for 4 h. After cooling down to RT, the obtained orange dispersion was washed with acetone and ethanol three times and the obtained powder was calcined at 450 °C for 4 h.

2.5. Photocatalytic activity test

This study focused on the application of BFO, BVO and BFO/BVO NCs as efficient photocatalysts for the rapid degradation of TC from aqueous solution. Aqueous suspensions (100 mL) containing 0.065 mg of BFO, BVO or BFO/BVO and 25 mg L⁻¹ of TC in 250 mL Erlenmeyer flasks were prepared. Then, the glass reactor was illuminated with a 55-W fluorescent lamp with an emission peak at 550 nm under continuous magnetic stirring. The distance between the solution and the lamps was approximately 30 cm. The solution temperature was kept between 28 - 30 °C by using a water bath. Before the light irradiation, the solutions were magnetically stirred in a dark place for 45 min, and the resulting suspension was placed in the presence of visible light for different time intervals. At each designated time

interval, 4 mL of the reaction solution was sampled and the liquid phase was easily separated from the photocatalyst. The absorption of the solution was converted to the TC concentration by using the standard curve.

Other experiments were also carried out by adding HCl or NaOH to the reaction solution to investigate the pH effects for TC photodegradation under different pHs.

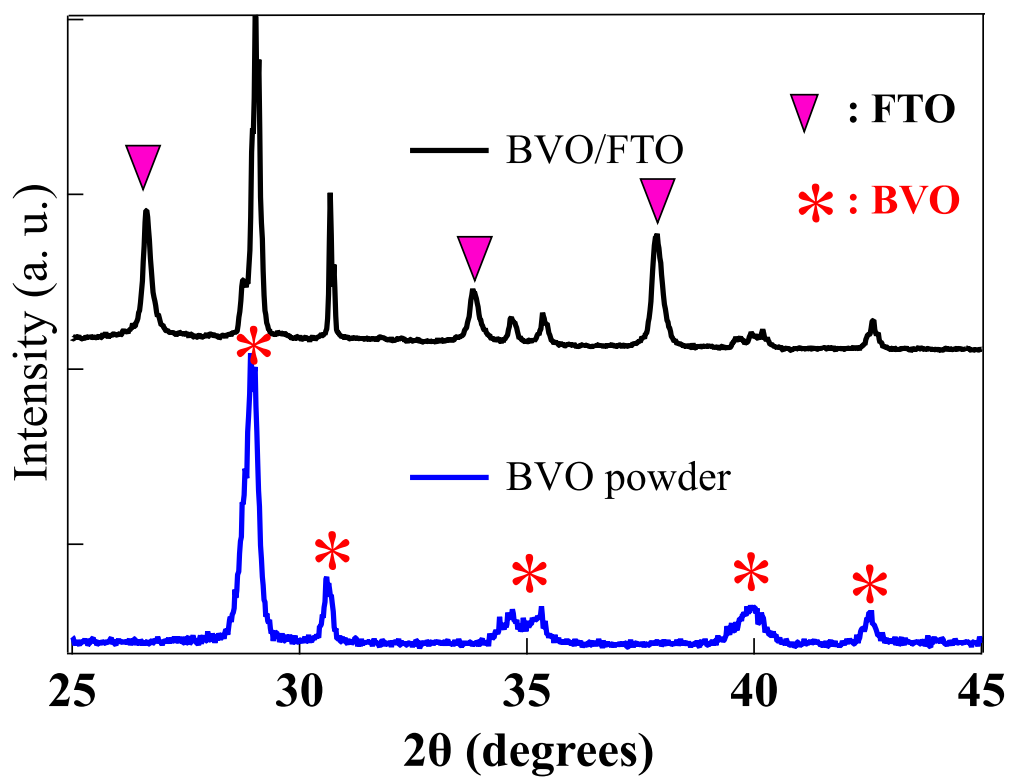


Fig. S1: XRD patterns of BVO powder and BVO/FTO electrode.

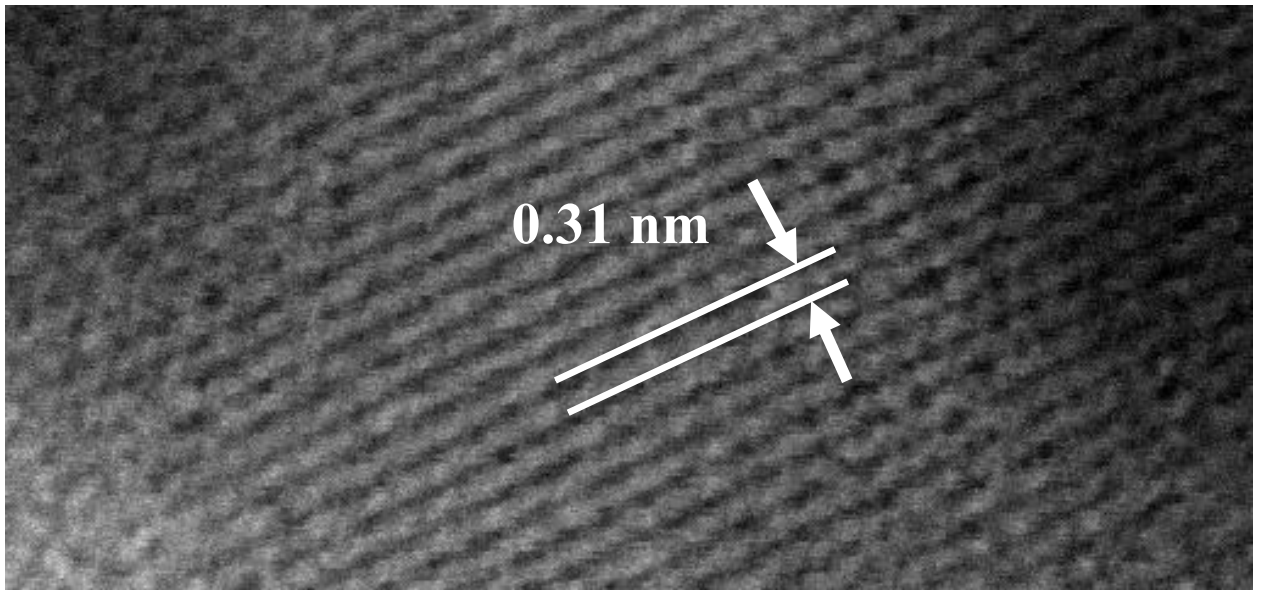


Fig. S2: HRTEM image of BiVO₄.

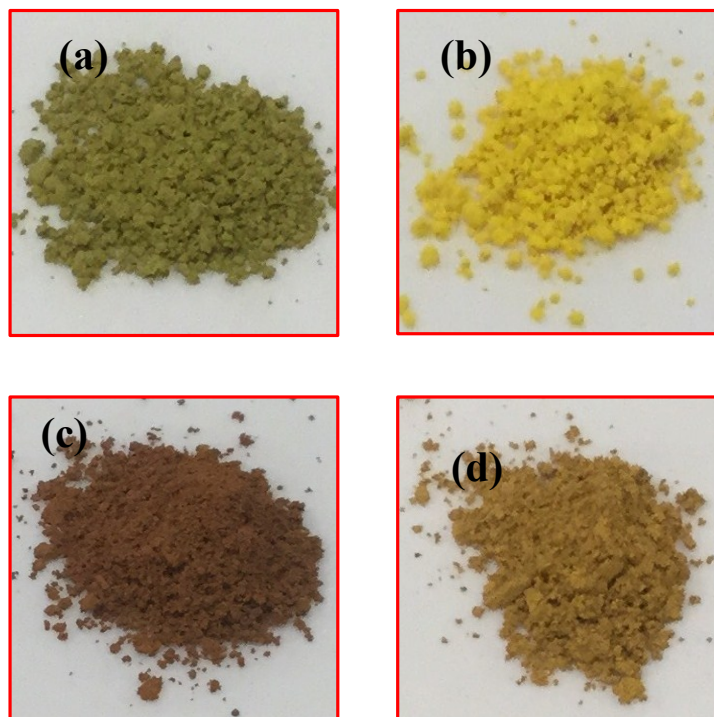


Fig. S3. Photographs of (a): BVO (before calcination), (b): BVO (after calcination), (c): BFO and (d): BVO/BFO.

The high resolution XPS spectra for Fe 2P core-level at room temperature for BVO and BVO/BFO are shown in Fig. S4.

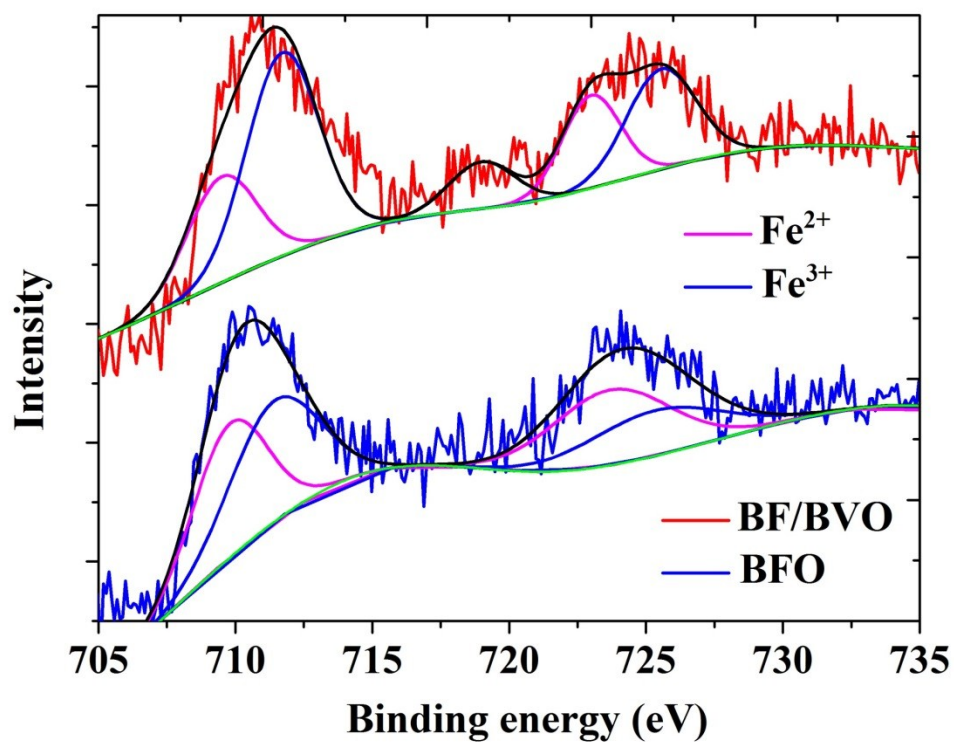


Fig. S4. High resolution XPS spectra for Fe 2P core-level at room temperature.

Fig. S5 displays the Raman spectra of BFO, BVO and BFO/BVO NCs. In BFO, the Raman active modes with A_1 and E symmetry can be assigned at 171, and 218 cm^{-1} , respectively. It is reported that Raman bands around 209, 323, 366, and 826 cm^{-1} are the typical vibrational bands of BVO. In the monoclinic phase of BVO, the peaks centered at 323 and 366 cm^{-1} were attributed to the typical antisymmetric and symmetric bending vibration modes of VO_4^{3-} , respectively. The weak Raman bands detected at 702 cm^{-1} was assigned to the long (A_g) asymmetric V-O stretching modes. An intense Raman band at 826 cm^{-1} was also detected and was assigned to the shorter symmetric V-O stretching mode (A_g). In addition, symmetric and asymmetric bending modes of the VO_4^{3-} tetrahedron were observed at 367 and 327 cm^{-1} , respectively. These Raman spectrum results shown in Fig. 1(d) for BFO/BVO NCs confirm the coexistence of nanocrystalline BFO and BVO in the BFO/BVO NCs.

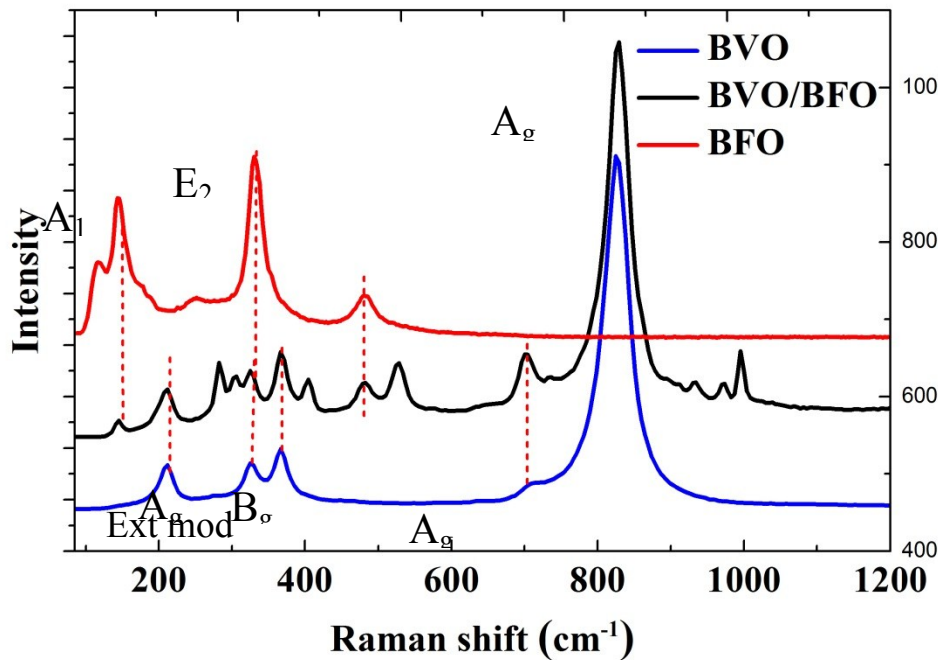


Fig. S5. Raman spectra of the as-synthesized BFO, BVO and BVO/BFO.

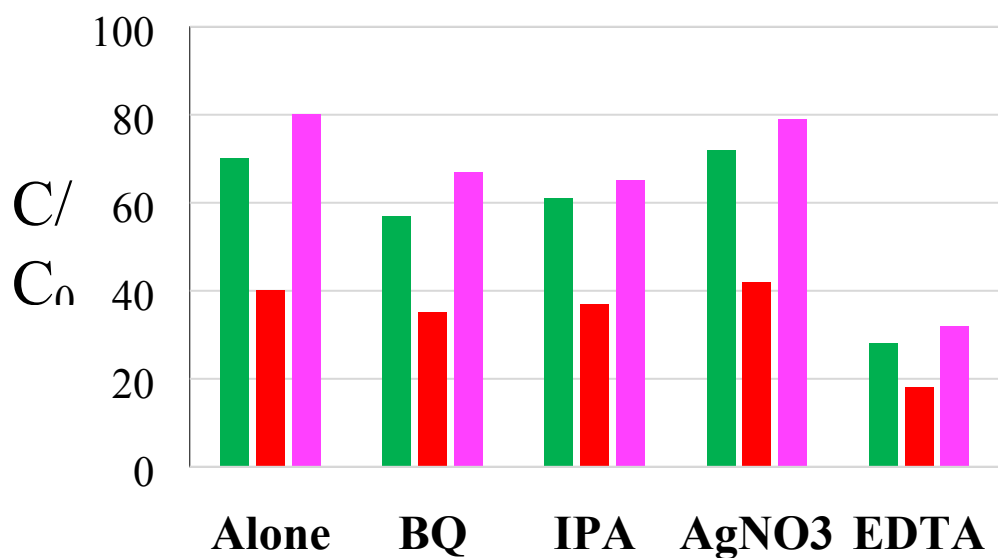


Fig S6: Photocatalytic degradation of TCs over different samples alone, and with the addition of different types of active species scavengers (i.e., AgNO₃, EDTA, TBA and BQ).

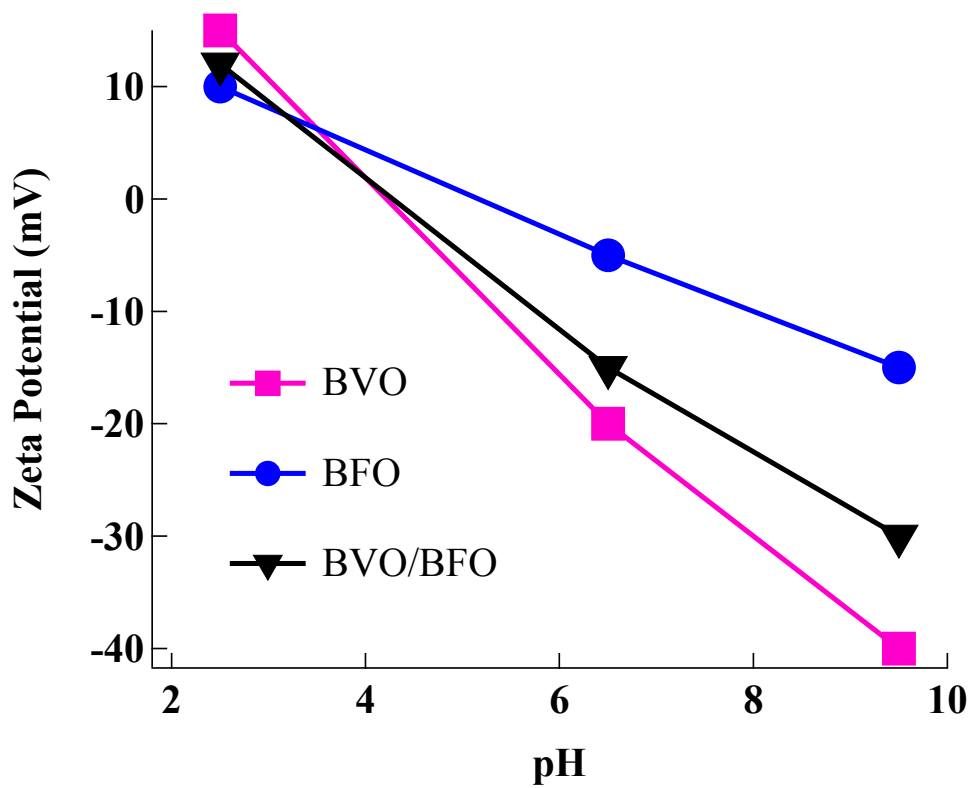


Fig S7: Surface charge measurement for 1mg/mL of catalysts in water at different pH values.

Synergism Calculation for TCs photodegradation:

Table S1: Photodegradation efficiency (%) of TCs for catalysts under different pH values				
Catalysts	TCs photodegradation efficiency BVO	TCs photodegradation efficiency BFO	TCs photodegradation efficiency BFO/BVO	
			Theoretical	Experimental
pH=2.5	43%	70%	56%	68%
pH=6.6	70%	40%	55%	70%
pH=9.5	85%	10%	48%	75%

We calculate the expected values of TCs photodegradation based on this fact that BVO and BFO has equal portion in BVO/BFO (1:1). Because we mixed starting materials with equal portion for both BVO and BFO. Therefore, we can suppose that the photodegradation efficiency of BVO/BFO can be obtained by:

$$\begin{aligned}
 & \text{TCs photodegradation efficiency of BVO/BFO,} \\
 & = 0.5 \times \text{TCs photodegradation efficiency of BVO} + 0.5 \\
 & \times \text{TCs photodegradation efficiency of BFO}
 \end{aligned}$$

$$\begin{aligned}
 \text{pH} = 2.5 & \Rightarrow \begin{cases} \text{Theoretical BFO / BVO}(1:1) = 0.5 \times 70\% + 0.5 \times 43\% = 56\% \\ \text{Experimental BFO / BVO} = 68\% \end{cases} \\
 \text{pH} = 6.6 & \Rightarrow \begin{cases} \text{Theoretical BFO / BVO}(1:1) = 0.5 \times 40\% + 0.5 \times 70\% = 55\% \\ \text{Experimental BFO / BVO} = 70\% \end{cases} \\
 \text{pH} = 9.5 & \Rightarrow \begin{cases} \text{Theoretical BFO / BVO}(1:1) = 0.5 \times 10\% + 0.5 \times 85\% = 48\% \\ \text{Experimental BFO / BVO} = 75\% \end{cases}
 \end{aligned}$$

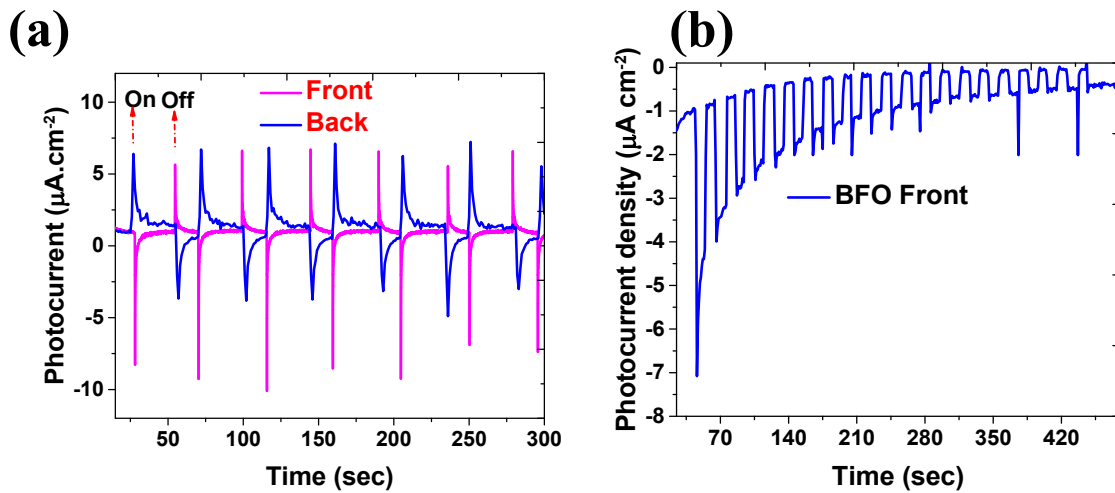
Photoelectrochemical properties of BFO:

Fig. S8 summarized the results of different PEC measurements for the BFO electrode in 0.5 M Na₂SO₄ under visible-light irradiation (250 W.cm⁻²). Fig. S8 (a) shows the photocurrent as a function of time under pulse irradiation for BFO as a working electrode under back- and front-side illuminations at an applied potential of 1.0 V vs. Ag/AgCl. As shown in Fig. S8 (a), an anodic or cathodic photocurrent response was observed for BFO from the back- or front-side illumination, respectively. n- and p-type semiconductors act as a photoanode and a photocathode, respectively. Thus, BFO thin films present an n-type behavior when illuminated from the back side but a p-type behavior when illuminated from the front side. Fig. S8b shows that the cathodic photocurrent of BFO from the front-side illumination at applied potential of 1 V vs. Ag/AgCl was diminished substantially in a very short irradiation time until it reached the plateau of the photocurrent, which is consistent with another relevant observation. Thus, it can be concluded that although the pure BFO electrode does not show good photocathode properties, it plays an important role in the electron-hole separation process by transferring the generated electrons and holes. Furthermore, due to the smaller band gap, it more likely increases the population of carriers in the electrode.

Here we discuss the higher photocurrent density of BVO/BFO in the back-side illumination compared to the front-side illumination as shown in Figure S8c. As we discussed in the previous paragraph, in the back-side illumination BFO acts as n-type catalyst while it acts as p-type electrode in the front-side illumination (Figs. S8 a and b). Then, in BFO/BVO electrode two different arrangements can be defined: 1) n-n junction in the back-side illumination, and 2) p-n junction in the front-side illumination.

In the back-side illumination as shown in Figure S8c, both BVO and BFO act as n-type semiconductors. The photogenerated holes in BVO move to BFO layer and then the holes transfer to FTO. Similarly to BVO, in BFO the photogenerated hole and electrons move in the same direction. However, in the BFO-BVO junction, the photogenerated holes of BVO and electrons of BFO can meet each other.

In the front-side illumination, the photogenerated electrons and holes in BFO/BVO move in the opposite direction as shown in the schematic of Fig. S8c. Therefore, the photogenerated holes in the junction interface of BFO and BVO are accumulated and act as recombination centers for electrons. These accumulated holes attracted the photogenerated electrons in BVO, increasing the recombination rate in BFO/BVO electrode in the front-side illumination with decreasing the photocurrent density.



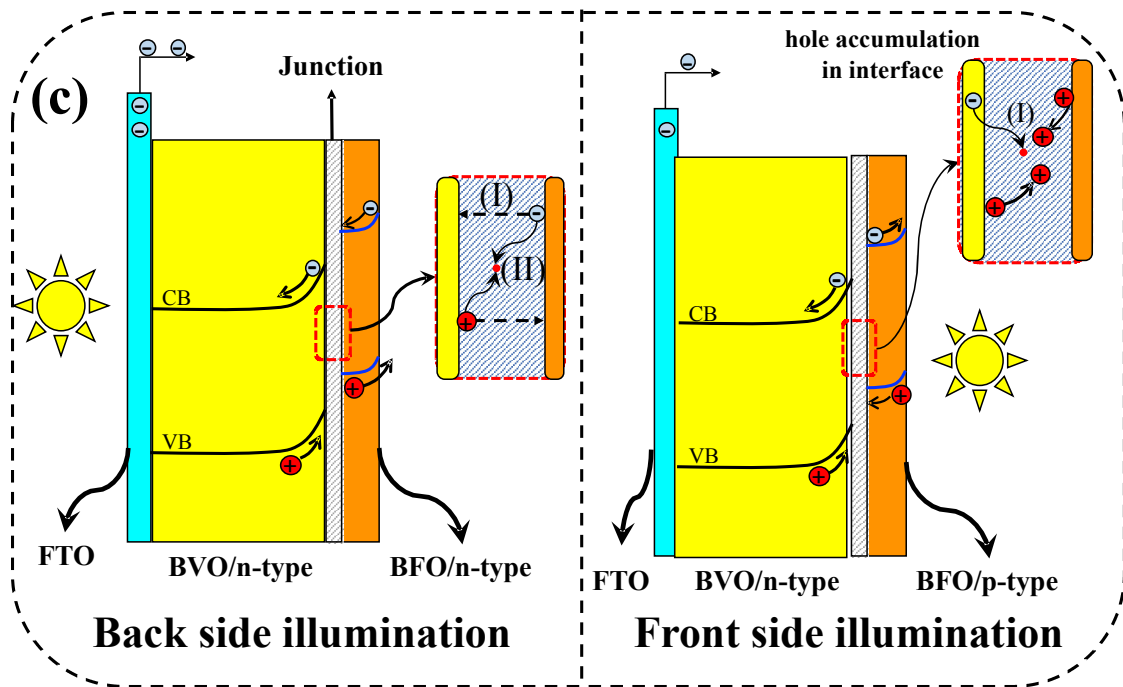


Fig. S8. (a) photocurrent vs time for BFO electrodes in back-side and front-side illumination, (b) Chronoamperometry of BFO electrode at applied potential of 1V vs Ag/AgCl at 0.5 M Na₂SO₄ solution, and (c) Schematic illustration of photogenerated electron-hole transfer within BVO/BFO electrode in back-side and front-side illumination.

Mott-Schottky equation and constant volume:

$$\frac{1}{C^2} = \frac{2}{\epsilon\epsilon_0 A^2 e N_D} (V - V_{fb} - \frac{K_B T}{e})$$

$$Slope = \frac{2}{\epsilon\epsilon_0 A^2 e N_D} \rightarrow N_D = \frac{2}{\epsilon\epsilon_0 A^2 e (Slope)}$$

$$V_{fb} = \text{int except} - \frac{K_B T}{e} \rightarrow \text{int except} = V_{fb} + \frac{K_B T}{e}$$

$$\epsilon = 68 \text{ for BVO}$$

$$\epsilon_0 = 8.854 * 10^{-12} F.m^{-1}$$

$$e = 1.6 * 10^{-19} C$$

$$K_B = 1.381 * 10^{-23} J.K^{-1}$$

$$T = 298K$$

Table S2: Previous research regarding photoelectrochemical properties of BVO/BFO heterojunction.

Photo-catalyst(Photoanode)	Method	Light source (Power type)	Electrolyte	Photocurrent density(1.23 V vs. Ag/AgCl)	Year of publication / Reference
BiVO ₄ /BiFeO ₃ photoanode	Spin coated	AM 1.5G simulated sunlight,	Na ₂ SO ₄ solution (0.5 M)+ H ₂ O ₂	0.6 mA cm ⁻²	2016/[1]
BiFeO ₃ /BiVO ₄ p-n heterojunction	Drop-casted	250 W Xe lamp	0.1 M Na ₂ SO ₄	0.2 mA cm ⁻²	2018/[2]
BiFeO ₃ photoanode	Pulsed laser deposition	150 W Xenon lamp	0.5 M aqueous Na ₂ SO ₄ (pH = 5.67)	0.06 mA cm ⁻²	2016/[3]
BiVO ₄	Dip coating	150 W Xenon lamp	0.5 M Na ₂ SO ₄	0.08 mA cm ⁻²	2019/[4]
BVO/BFO	Drop-casted	150 W Xenon lamp	0.1 M Na ₂ SO ₄	0.3 mA cm ⁻²	Our work

Reference:

- [1] J. Xie, C. Guo, P. Yang, X. Wang, D. Liu, C.M. Li, Bi-functional ferroelectric BiFeO₃ passivated BiVO₄ photoanode for efficient and stable solar water oxidation, *Nano Energy*, 31 (2017) 28-36.
- [2] T. Soltani, A. Tayyebi, B.-K. Lee, BiFeO₃/BiVO₄ p– n heterojunction for efficient and stable photocatalytic and photoelectrochemical water splitting under visible-light irradiation, *Catalysis Today*, (2018).
- [3] J. Song, T.L. Kim, J. Lee, S.Y. Cho, J. Cha, S.Y. Jeong, H. An, W.S. Kim, Y.-S. Jung, J. Park, Domain-engineered BiFeO₃ thin-film photoanodes for highly enhanced ferroelectric solar water splitting, *Nano Research*, 11 (2018) 642-655.
- [4] M. Tayebi, A. Tayyebi, B.-K. Lee, Improved photoelectrochemical performance of molybdenum (Mo)-doped monoclinic bismuth vanadate with increasing donor concentration, *Catalysis Today*, 328 (2019) 35-42.